1   Introduction

Modeling liquid water at interfaces with molecular dynamics (MD) simulations is a means in understanding interfacial processes in catalysis and electrochemistry. Up to now this has been mostly done without incorporating the molecular polarizability of the water molecules. Recently developed polarizable water models raise the question whether these models lead to a more accurate simulation of water at interfaces.

Incorporating molecular polarizability into a water model enables the molecules to react to local perturbations in the electrostatic field. For the simulations of bulk system one can assume, that these perturbations will be averaged out and so applying a less time consuming and easier to handle nonpolarizable water model will be sufficient in most cases. At interfaces however there will be generally an anisotropic electrostatic field, even after averaging out the local perturbations. To prove how far this anisotropy affects the properties of the interfacial water molecules one can compare the results of MD simulations which use a polarizable water model with the results of simulations of the same system with a nonpolarizable water model which employs the same geometry.

To-date, only a few simulations of aqueous interfaces using polarizable water models have been reported. Wallqvist [1] /a0057/ has simulated polarizable water on a hydrophobic wall, Zhu and Robinson [2] /a0024/ investigated polarizable water between charged and uncharged rigid wall, and Motakabbir and Berkowitz [3] /a0058/ examined the liquid/vapor interface. Whereas neither Wallqvist nor Motakabbir and Berkowitz found any substantial differences between simulations with polarizable and nonpolarizable water, Zhu and Robinson reported changes in the dynamic and the structural properties due to the inclusion of the molecular polarizability of

the water molecules.

In this study we will present molecular dynamics simulations of a thin water film adsorbed on a model surface which, in some respect, resembles *fcc*-Ni(100), and of a water lamina confined between two *bcc*-Hg(111) surfaces. In both cases we will compare the results of simulations using the (nonpolarizable) TIP4P model [4] **/a0033/** with simulations using a polarizable water model [5] **/dipl/**, which is derived from the TIP4P-FQ model introduced by Rick *et al.*[6] **/a0027/**.

2   Models

In this study we examined two model systems with different approaches for modeling the metal surfaces. The first system, which we will refer to as system I, is a thin water film consisting of 200 water molecules in a rectangular box with the dimensions $L_x = L_y = 18$ Å and periodic boundary conditions in $x-$ and $y-$direction. The film is in contact with a corrugated external potential which is composed of a Morse function, a corrugation term for oxygen-surface and a repulsive term for hydrogen-surface interactions:

$$V_{\text{water}-\text{surface}} = V_O(x_O, y_O, z_O) + V_H(z_{H1}) + V_H(z_{H2})$$

with

$$
\begin{aligned}
V_O(x, y, z) \;=\; & D_O \left[\exp(-2\beta_O(z - z_1)) - 2 \cdot \exp(-\beta_O(z - z_1)) \right] \\
& + \; \alpha \cdot D_O \exp(-2\beta_O(z - z_1)) \cdot \left[\cos\left(\frac{10\pi x}{L_x}\right) + \cos\left(\frac{10\pi y}{L_y}\right) \right]
\end{aligned}
$$

and

$$V_H(x, y, z) = \gamma \cdot D_O \exp(-2\beta_H(z - z_2)) \,.$$

Using the following parameters $D_O = 30$ kJ/mol, $\alpha = 0.1$, $\gamma = 0.2$, $z_1 = 0$ Å, $z_2 = -4$ Å, $\beta_O = \beta_H = 1$ Å^{-1} the corrugation (described by the parameter α) is felt only in the repulsive part of the Morse potential function and has a periodicity of 3.6 Å in both directions parallel to the surface, thus roughly corresponding to the periodicity on a Ni(100) surface. A more detailed description and examination of this interface can be found in reference [7] **/eckhard-zakopane/**. The metallic properties of the surface are modeled through image charges.

The second model, which we will call system II, is a water lamina between two mercury crystals with *bcc*-(111) surface geometry. The lamina is consists of 252 water molecules in a rectangular box with the length of 18 Å in x-direction and 15.58845 Å in y-direction and standard periodic boundary conditions in these directions. The water mercury potential was derived from *ab initio* SCF calculations of water mercury clusters [8, 9] **/e1799,a0066/**. The employed potential functions for the mercury oxygen and the mercury hydrogen interactions were

$$
\begin{aligned}
V_{\text{Hg}-\text{O}}(r, \rho) &= \left[25518 \times \exp(-2.0829r) - 5508.2 \times \exp(-1.3922r)\right] f(\rho) \\
&\quad + 8813.2 \times \exp(-2.1759r) \left[1 - f(\rho)\right] \\
V_{\text{Hg}-\text{H}}(r, \rho) &= 2603.6[\exp(-2.2230r) + \exp(-2.6737r)] \\
&\text{with} \\
f(\rho) &= \exp(-0.2213\rho^2), \\
&\text{and} \\
\rho &= \sqrt{\Delta x^2 + \Delta y^2}
\end{aligned}
$$

for energies in kJ/mol and distances in Å. For more information on this system see reference [9] **/a0066/**.

For both systems, MD simulations with the TIP4P model were performed.

Then, the simulations with the polarizable water model (see below), were started from the final, well-equilibrated configurations of these runs. All simulations were performed at 300±5 K using the SHAKE version of the Verlet algorithm [10] **/allenutild/** for integrating the equations of motion. The long ranged electrostatic interactions were handled with two-dimensional tabulated Ewald-summation. Table 1 gives a summary of the performed simulations.

Table 1:

Nr.	system	N_{water}	water model	length of the simulation		LRC
1	I	200	TIP4P	160,000 × 2.5 fs =	400 ps	Ewald
2	I	200	polarizable	28,000 × 2.5 fs =	70 ps	Ewald
3	II	252	TIP4P	57,600 × 2.5 fs =	144 ps	Ewald
4	II	252	polarizable	18.000 × 2.5 fs =	45 ps	Ewald
5	bulk	216	polarizable	37,500 × 2.0 fs =	75 ps	ShFo

Table 1: Overview of the performed simulations. N_{water} stands for the number of water molecules in the simulation cell. LRC stands for the method used for handling the long range Coulomb interactions: Ewald = 2D-Ewald summation, ShFo = shifted force smooth truncation.

The polarizable water model we used in this study is derived from the TIP4P-FQ model by Rick *et al.*[6] **/a0027/**. It features the standard TIP4P geometry [4] **/a0033/**, a Lennard-Jones potential energy term between the oxygen atoms and Coulomb interactions between the three charged sites. Unlike in the standard TIP4P model and like in the TIP4P-FQ model the charges have to be recalculated in every time step with respect to the local electrostatic field. The total charges are composed of two contributions: a constant part which represents the permanent dipole moment of the water molecule and a fluctuating part which models the induced dipole mo-

ment. For a more detailed description see reference [6] **/a0027/**. In contrast to Rick *et al.* we used a self-consistent iteration scheme instead of the extended Lagrangian method to calculate the charges. To verify the model an MD simulation of bulk water (216 molecules in a cubic box with an edge length of 18.62 Å and periodic boundary conditions in all three directions) has been performed. The shifted force method was used to handle long range Coulomb interactions and the equations of motion were integrated using the Verlet algorithm. The simulation lasted for a total of 80 ps with an integration time step of 2 fs. As proof of the model we compared the pair correlation functions to those of previous TIP4P simulations of bulk water [5] **/dipl/**. The corresponding pair correlation functions were nearly identical. This is consistent with the results of Rick *et al.*[6] **/a0027/** and therefore a detailed presentation of the results of this simulation is omitted. The only noticeable difference to that work we found was that the average total dipole moment is only 2.31 D compared to 2.62 D for the TIP4P-FQ model. Taking into account the dipole moment which has been calculated for ice, 2.6 D, [11] **/a0067/** and the generally expected dipole moment of liquid water at room temperature, 2.4-2.5 D, the average dipole moment for this model is, although higher than that of the TIP4P (2.18 D) [4] **/a0033/**, too small. On the contrary other simulations of polarizable water [6, 12, 13, 14, 15, 16, 17] **/a0027,a0035,a0029,a0053,a0037,a0013,a0023/** yield average dipole moments of 2.6-3.2 D, which are higher than the expected values. Therefore we did not consider this a problematic property of the polarizable water model, especially as the liquid structure expressed by the pair correlation functions was in good agreement with the results of the TIP4P simulations.

3 Results

System I - water film at a corrugated surface
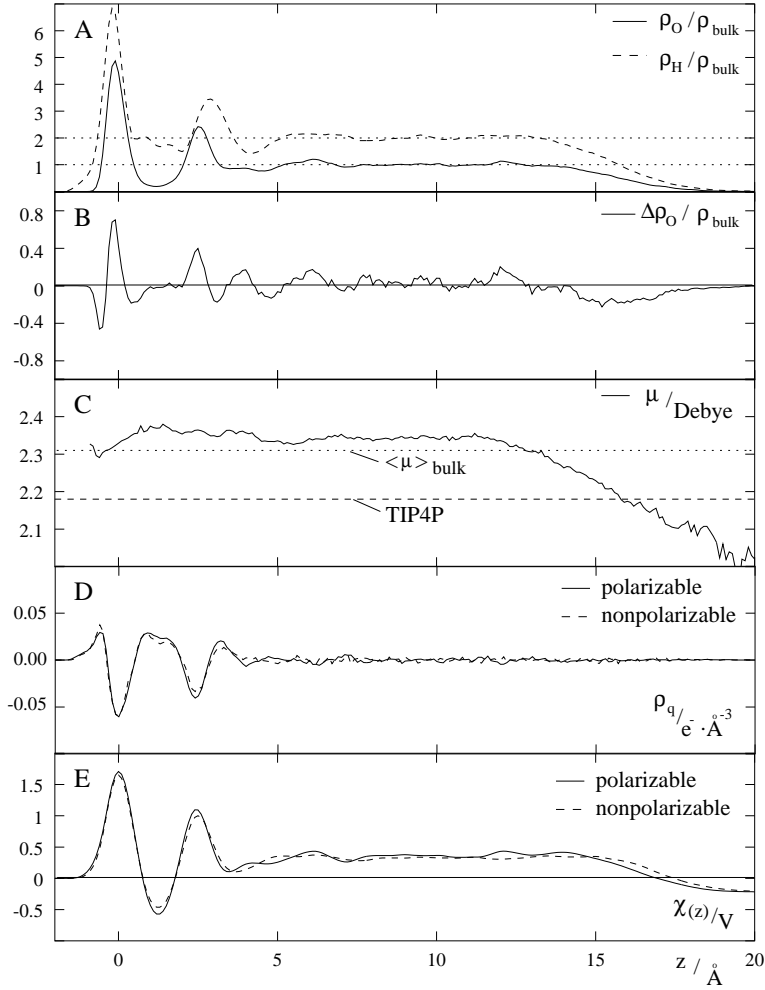
Figure 1:

Figure 1: Simulation of a water film at a corrugated model surface.

A) Oxygen (solid) and hydrogen (dashed) density profiles for polarizable water model. The dotted lines represent the bulk-densities. B) Difference between the oxygen density of the simulation using the polarizable and the simulation using the nonpolarizable water model. $\Delta\rho_O = \rho_{O,\mathrm{polarizable}} - \rho_{O,\mathrm{TIP4P}}$ C) Distribution of the

average dipole moment along the z-axis (solid line) compared to the average dipole moment for polarizable bulk water (System dotted line) and the dipole moment of the TIP4P model (dashed line). D) Oxygen charge density for the polarizable (solid line) and the nonpolarizable (dashed line) water model. E) Electrostatic potential profile for the polarizable (solid line) and the nonpolarizable (dashed line) water model.

Figure 1 shows the distribution along the z-axis of some properties of system I. In figure 1A the oxygen (solid line) and hydrogen (dashed line) density profiles for the simulation using the polarizable water model (No. 2, see table 1) are presented. The shape of both distributions is typical for a water film on a metallic surface with one sharp maximum (for this simulation at $z = 0$ Å) which represents the first absorbed layer of water molecules and a second, broader maximum (here for z between 2 and 4 Å) representing a second, less pronounced layer of molecules. For z between 5 and 12 Å the density is bulk-like and for $z > 12$ Å it decreases to zero. To stress the changes from the simulation using the non-polarizable to the simulation using the polarizable water model the difference of the oxygen densities ($\Delta\rho_O = \rho_{O,\text{polarizable}} - \rho_{O,\text{TIP4P}}$) has been calculated and is presented in figure 1B (solid line). The maximum and the neighboring two small minima at about $z = 0$ Å indicate, that the first layer of oxygen atoms is more pronounced for the polarizable model than for TIP4P. Furthermore the minimum at $z > 14$ is a signal, that the water film is smaller and thus of higher density when using the polarizable water model. In the next plot (figure 1C) the average total dipole moment of the water molecules with respect to their distance to the surface (solid line) is compared to the average dipole moment calculated from the bulk water simulation (No. 5, dotted line) and the dipole moment of the TIP4P model (dashed line). Whereas the mean dipole moment does not change by more

than 5 % for the metal/water interface, it decreases continuously to the gas phase value (1.85 D) with the decreasing density (for $z > 12$ Å). This continuous decrease illustrates how, by design, a polarizable water model is able to reflect the transition of the electrostatic properties from liquid state to gas phase. A consequence of the decreasing dipole moment is, that because of the weaker Coulomb interactions the water/vacuum interface broadens. This can be proved by examining the steepness of the density decay at the interface. Figure 2 shows the oxygen densities for the polarizable (solid line) and the nonpolarizable (dashed lines) water model at the water/vacuum interface (for 14 Å $> z >$ 18 Å and relative densities between 0.1 and 0.9).
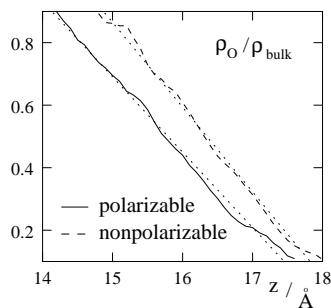
Figure 2:

Figure 2: Excerpt of the oxygen density distribution from the simulation system I with the polarizable and the nonpolarizable TIP4P model.

Fitting the data to linear equations yields

$$y = -0.24 \times z + 4.31$$

for the polarizable and

$$y = -0.27 \times z + 4.93$$

for the nonpolarizable model (dotted lines in figure 2). Thus the oxygen density decay is roughly 12 percent faster for the nonpolarizable water model.

Furthermore the total dipole moment in the center of the bulk-like region of this system is about 0.05 Debye higher than the value we calculated from

the bulk water simulation (No. 5, dotted line). Figure 1D shows the charge densities for the simulations with polarizable water (solid line) and TIP4P (dashed line). The differences between the two plots are very small. From the charge densities the electrostatic potential profiles $\chi(z)$ have been calculated. This was done by solving the one-dimensional Poisson equation,

$$\chi(z) = -\int\limits_{-\infty}^{z} \rho_q(z')(z-z')\mathrm{d}z'$$

where ρ_q is the charge density. Like for the charge densities, the differences between the two models are small (see figure 1E).

System II - water lamina between mercury crystals

Figure 3: Simulation of a water lamina between two mercury crystals.

A) Oxygen (solid) and hydrogen (dashed) density profiles for polarizable water model. The dotted lines represent the bulk-densities. B) Difference between the oxygen densities of the simulation using the polarizable and the simulation using the nonpolarizable water model. $\Delta\rho_O = \rho_{O,\mathrm{polarizable}} - \rho_{O,\mathrm{TIP4P}}$ C) Distribution of the average dipole moment along the z-axis (solid line) compared to the average dipole moment for polarizable bulk water (dotted line) and the dipole moment of the TIP4P model (dashed line). D) Oxygen charge density for the polarizable (solid line) and the nonpolarizable (dashed line) water model. E) Electrostatic potential profile for the polarizable (solid line) and the nonpolarizable (dashed line) water model.

Figure 3 shows, analogous to figure 1, distributions along the z-axis for the simulation of System II. The figure is organized in the same manner as figure 1. so there are the oxygen (solid line) and hydrogen (dashed line) densities in figure 3A, the difference between the oxygen densities for polarizable

Figure 3:
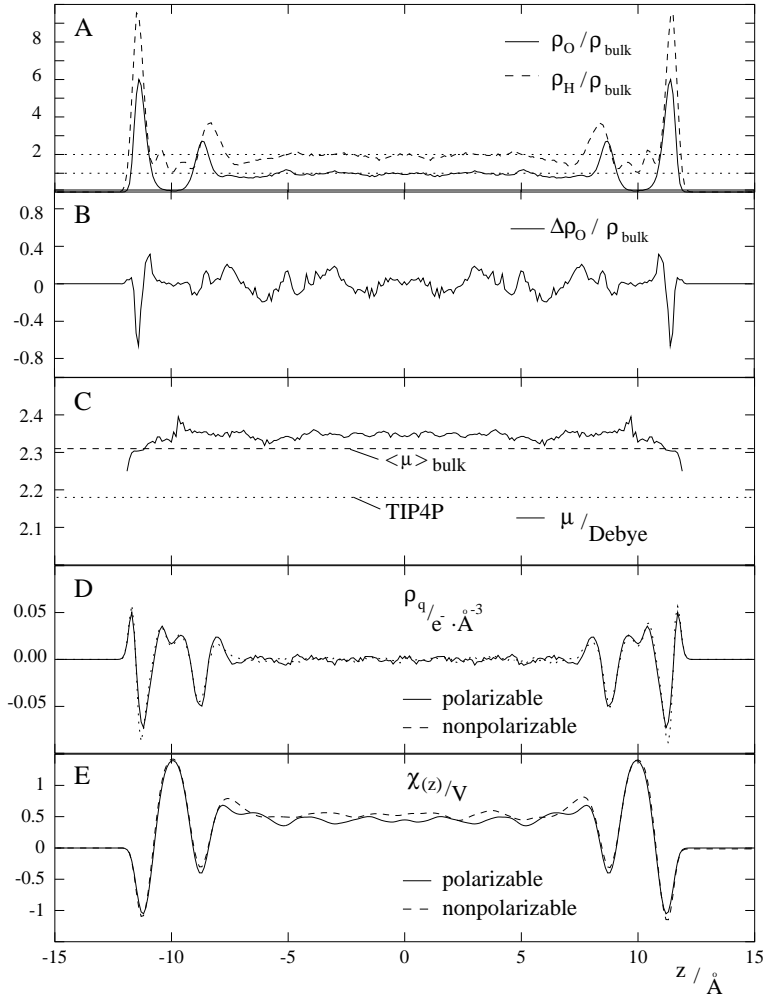
and nonpolarizable TIP4P, the average total dipole moment compared to the average bulk value and the non-polarizable TIP4P value in figure 3C, the charge density distributions in figure 3D and the electrostatic potential profiles $\chi(z)$ in figure 3E. Like in the simulation of system I, the oxygen and hydrogen density profiles (figure 3A) reveal two layers of water molecules neighboring the metal surface and a bulk-like region. Furthermore the distribution of the oxygen density difference (see figure 3B) has the most significant feature at $\pm$ 11.5 Å, which is the first layer of oxygen atom. But in contrast

to the water/model-metal interface the oxygen peak is broadened for the polarizable model compared to the TIP4P model. Without the free surface the total dipole moment (figure 3C) does not undergo major changes. Only for water molecules in the first layer on the mercury surface the average dipole moment drops from more than 2.35 D to approximately 2.25 D. This is another similarity to the water/metal interface of system I. In addition to that the average total dipole moment in the bulk region is also slightly enhanced compared to the average bulk dipole moment for the same polarizable water model. And at last the charge density distributions (figure 3D) and the potential drops (figure 3E) are nearly the same for both models, which is comparable to system I, too.

Discussion

With the exception of the water/vacuum interface where - as a result of the design of the polarizable water model - the electrostatic interaction for the polarizable water model differ greatly from the bulk-like regions, the effect of including the polarizability into the TIP4P model are small. For both examined solid/water interfaces the average total dipole moment of water molecules in the interface region does not differ very much compared to molecules of the bulk-like region. As the polarizable water model was designed to reproduce the properties of the TIP4P model in bulk water, these observations lead to the conclusion conclude, that the benefit of simulating the interface between liquid water and solid metals with a polarizable water model instead of a nonpolarizable one is very small. This agrees with the observations of Wallqvist [1] **/a0057/**. The changes for the total dipole moment in the region of the water/metal interface were even smaller than for the water film between hydrophobic walls, Wallqvist has investigated. We found

no evidence for substantial changes of dynamic and structural properties as reported by Zhu and Robinson [2] **/a0024/**. But these may be an effect of using plates or charged plates as a model for a metal surface.

We found the most noteworthy changes introduced by the polarizable water model for the liquid/vapor interface. There the mean dipole moment of the water molecules drops continuously from the bulk value to the gas phase value. The weakening Coulomb interactions results in a significantly broadened interface. Therefore we conclude that a polarizable water model will be of most use when liquid/vacuum interface is the matter of interest.

References

[1] A. Wallqvist, Chem. Phys. Lett. **165**, 437 (1990).

[2] S. B. Zhu and G. W. Robinson, J. Chem. Phys. **94**, 1403 (1991).

[3] K. A. Motakabbir and M. L. Berkowitz, Chem. Phys. Lett. **176**, 61 (1991).

[4] W. L. Jorgensen *et al.*, J. Chem. Phys. **92**, 926 (1983).

[5] A. Kohlmeyer, Diplomarbeit, Universität Ulm, 1995.

[6] S. W. Rick, S. J. Stuart, and B. J. Berne, J. Chem. Phys. **101**, 6141 (1994).

[7] E. Spohr, J. Mol. Liquids **64**, 91 (1995).

[8] R. R. Nazmutdinov, M. Probst, and K. Heinzinger, J. Electroanal. Chem. **369**, 227 (1994).

[9] J. B"ocker, R. Nazmutdinov, E. Spohr, and K. Heinzinger, Surf. Sci. **335**, 372 (1995).

[10] M. Allen and D. Tildesley, *Computer Simulation of Liquids* (Clarendon Press, Oxford, 1987).

[11] C. A. Coulson and D. Eisenberg, Proc. Roy. Soc. **A. 291**, 445 (1966).

[12] K. Watanabe and M. L. Klein, Chem. Phys. **131**, 157 (1989).

[13] G. Ruocco and M. Sampoli, Mol. Phys. **82**, 875 (1994).

[14] M. Sprik and M. L. Klein, J. Chem. Phys. **89**, 7556 (1988).

[15] M. Sprik, J. Phys. Chem. **95**, 2283 (1991).

[16] D. van Belle, M. Froeyen, G. Lippens, and S. J. Wodak, Mol. Phys. **77**, 239 (1992).

[17] P. Ahlström, A. Wallqvist, S. Engström, and B. Jönsson, Mol. Phys. **68**, 563 (1989).